

Experimental Study of Gaseous Elemental Mercury Removal with $\text{CeO}_2/\gamma\text{-Al}_2\text{O}_3$

Xiaoyu Wen,^{†,‡} Caiting Li,^{*,†,‡} Xiaopeng Fan,^{†,‡} Hongliang Gao,^{†,‡} Wei Zhang,^{†,‡} Ling Chen,^{†,‡} Guangming Zeng,^{†,‡} and Yapei Zhao^{†,‡}

[†]College of Environmental Science and Engineering, and [‡]Key Laboratory of Environmental Biology and Pollution Control (Ministry of Education), Hunan University, Changsha 410082, People's Republic of China

ABSTRACT: The Hg^0 removal ability of $\gamma\text{-Al}_2\text{O}_3$ impregnated with cerium dioxide ($\text{CeO}_2/\gamma\text{-Al}_2\text{O}_3$) was tested in the experimental flue gas of $\text{N}_2 + \text{O}_2 + \text{NO} + \text{SO}_2 + \text{H}_2\text{O}$. Brunauer–Emmett–Teller (BET), X-ray diffractogram (XRD), and thermogravimetric (TG) analyses were used to characterize the samples. The effects of CeO_2 loading values, reaction temperatures, reaction time, and individual flue gas components, including SO_2 , NO , O_2 , and $\text{H}_2\text{O}(\text{g})$, on the Hg^0 removal efficiency were investigated. The results show that the Hg^0 removal efficiency of $\gamma\text{-Al}_2\text{O}_3$ can be greatly improved by CeO_2 and, at a test temperature of 350 °C, the best suitable loaded mass percentage of CeO_2 is 9%. In the temperature range from 150 to 350 °C, the Hg^0 removal efficiency using $\text{CeO}_2/\gamma\text{-Al}_2\text{O}_3$ increases with the increase of the temperature and then decreases above 350 °C, except virgin $\gamma\text{-Al}_2\text{O}_3$. In addition, the presence of O_2 and NO have positive effects on the Hg^0 removal efficiency, while the presence of SO_2 and H_2O inhibited it. Furthermore, prolonging the reaction time had a small negative effect on the Hg^0 removal performance, indicating that the catalyst of $\text{CeO}_2/\gamma\text{-Al}_2\text{O}_3$ possesses thermostability.

1. INTRODUCTION

Mercury has been a well-known environmental pollutant for several decades, because it has detrimental effects on human health and the environment because of its volatility, persistence, bioaccumulation, and toxicity.^{1–3} Consequently, mercury emissions are receiving more and more attention over recent years. The United Nations Environment Program⁴ proposed a global legally binding paper on mercury emissions in 2010, and global mercury pollution control is becoming a topic of increasing legislative and scientific focus.

According to refs 5–7, there are mainly three forms of mercury in coal-fired flue gas: elemental mercury (Hg^0), oxidized mercury (Hg^{2+}), and particle-bound mercury (Hg^{p}). Different forms of mercury have different physical and chemical properties. Specifically, Hg^{2+} is water-soluble and can be removed by the wet flue gas desulfurization (WFGD) system; Hg^{p} can be captured by a dust removal device, e.g., electrostatic precipitators (ESPs). However, in terms of Hg^0 , it is insufficiently captured because of its high volatility and low solubility in water. Hence, the study on Hg^0 removal from flue gas is becoming a scientific focus. Several methods, such as the particulate adsorption method, oxidation–reduction method, and chemical sedimentation method, have been proposed for control of Hg^0 emissions and evaluated from bench to pilot scale in the past few decades.^{8–11} Among those schemes, the major drawbacks of the particulate adsorbent are high costs, poor capacity, narrow temperature range of application, and slow regeneration and adsorption rates,¹² and therefore, the oxidation–reduction method exhibits a promising future. In this method, the catalyst is the most important element because it plays a dominant role in the operating costs and Hg^0 removal performance.

At present, many catalysts, such as $\text{V}_2\text{O}_5/\text{AC}$, MnO_2/AC , and $\text{Fe}_2\text{O}_3/\text{TiO}_2$, have been used in the oxidation–reduction

method and proven to be effective for Hg^0 removal.^{13–16} However, it was seldom reported that $\text{CeO}_2/\gamma\text{-Al}_2\text{O}_3$ was used as a catalyst in the Hg^0 oxidation–reduction or capture process. As reported, cerium oxide (CeO_2), as a nontoxic, abundant, and inexpensive rare earth material, attracted considerable attention for its potential application as fast ion conductors, oxygen-storage capacitors, catalysts, ultraviolet (UV) blockers, and polishing materials.^{17–19} Most importantly, it was also reported that CeO_2 can enhance the Hg^0 removal efficiency of many catalysts.^{20,21} Nevertheless, pure ceria has poor thermal stability, and it undergoes a rapid sintering at higher temperatures, thereby losing oxygen storage capacity (OSC), which would lead to the deactivation of the catalysts. Therefore, many efforts have been devoted to the chemical synthesis of metal oxides impregnated with CeO_2 . The mixing of two different oxides offers an opportunity not only to improve the performance of the involved metal oxide but also to form new stable compounds that may lead to totally different physicochemical properties and catalytic behavior from the individual components.²² $\gamma\text{-Al}_2\text{O}_3$ has important applications as an industrial catalyst support, catalyst, adsorbent, or ceramic raw material, because of its low costs, high surface area and porosity, good thermal stability, high mechanical strength, and extensive variability of acid–base properties.^{23–26} Hence, the major objective of present study is to perform an experimental study to investigate the Hg^0 removal using CeO_2 supported by $\gamma\text{-Al}_2\text{O}_3$ ($\text{CeO}_2/\gamma\text{-Al}_2\text{O}_3$) as the catalyst. Experimental studies were carried out on a lab-scale fixed-bed system. The simulated flue gas system included N_2 , O_2 , SO_2 , NO , H_2O , and gaseous Hg^0 . During the course of the study, different operating conditions, including loading values of CeO_2 , reaction

Received: January 25, 2011

Revised: May 24, 2011

Published: May 25, 2011

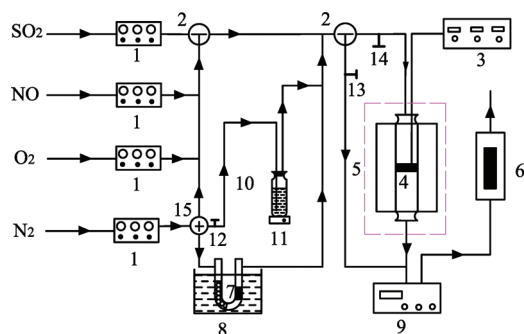


Figure 1. Flow diagram of the experimental setup for Hg^0 removal: (1) mass flow controller, (2) three-way valve, (3) temperature controller, (4) catalyst, (5) fixed-bed reactor, (6) exhaust gas collector, (7) Hg^0 permeation tube, (8) water bath, (9) Hg analyzer, (10) water bubbler, (11) heating plate, (12–14) valves, and (15) four-way valve.

temperatures, reaction time, and flue gas components on the removal efficiency were discussed.

2. EXPERIMENTAL SECTION

2.1. Catalyst Preparation. First, the commercially available $\gamma\text{-Al}_2\text{O}_3$ was ground, then washed with deionized water, and dried in an electric blast drying oven at $90\text{ }^\circ\text{C}$ for 24 h. After that, the sample was stored in a desiccator for future use.

Samples of $\gamma\text{-Al}_2\text{O}_3$ impregnated with CeO_2 (loading values were 3, 6, 9, 12, and 15 wt %) were prepared by the thermal decomposition of $\text{Ce}(\text{NO}_3)_3 \cdot 6\text{H}_2\text{O}$ loaded on $\gamma\text{-Al}_2\text{O}_3$ as follows: At first, $\text{Ce}(\text{NO}_3)_3 \cdot 6\text{H}_2\text{O}$ was dissolved in deionized water to form the solution. Then, $\gamma\text{-Al}_2\text{O}_3$ was added to the solution with stirring in a proportion corresponding to different loading values varied from 3 to 15 wt %. Next, the samples were dried in an electric blast drying oven at $100\text{ }^\circ\text{C}$ for 12 h. After this, the dried samples of $\text{CeO}_2/\gamma\text{-Al}_2\text{O}_3$ were calcined in a muffle furnace at $500\text{ }^\circ\text{C}$ for 4 h and then cooled to ambient temperature. At last, the samples were stored in a desiccator for future use.

2.2. Catalyst Characterization. X-ray diffractogram (XRD) measurements were carried out with a diffractometer to determine the crystal species distribution of the catalyst. The Rigaku Rotaflex D/Max-C system has Cu $K\alpha$ radiation as the X-ray source. The accelerating voltage and the applied current were 35 kV and 30 mA, respectively.

The Brunauer–Emmett–Teller (BET) theory was used to calculate the surface area, total pore volume, and pore size of the catalysts from the measured nitrogen adsorption isotherm at $-196\text{ }^\circ\text{C}$ obtained with a Micromeritics ASAP 2010 analyzer. All of the $\text{CeO}_2/\gamma\text{-Al}_2\text{O}_3$ powders were degassed at $120\text{ }^\circ\text{C}$ prior to BET measurements.

The thermogravimetric (TG) analyses of samples were performed with a TG analyzer (STA-409PC/PG). For each test, approximately 10 mg of sample was heated from 80 to $800\text{ }^\circ\text{C}$ at the heating rate of $10\text{ }^\circ\text{C min}^{-1}$.

2.3. Experimental Setup and Procedure. Research on the Hg^0 removal was carried out in a specially designed system (Figure 1). The simulated flue gas consisted of five major gases: SO_2 , NO , O_2 , N_2 , and H_2O . Thereinto, the N_2 flow was distributed into three branches. The first stream converged with the individual stream of SO_2 , NO , and O_2 and formed the main gas flow. The second N_2 stream passed through a heated water bubbler (10) (with an inner diameter of 5 cm) to introduce $\text{H}_2\text{O}(\text{g})$ into the simulated flue gas system. The third N_2 stream was used as Hg^0 -laden gas stream by passing through the Hg^0 permeation tube (7). To guarantee a constant permeation concentration, the Hg^0 permeation tube was placed in a U-shaped glass tube, which was immersed in a constant temperature ($45 \pm 0.5\text{ }^\circ\text{C}$) water bath (8). The gas flow rate was controlled in each experiment by mass flow

Table 1. Porous Structure Parameters of the Samples

sample	BET surface area (m^2/g)	total pore volume (cm^3/g)	pore size (nm)
$\gamma\text{-Al}_2\text{O}_3$	141.66	0.43	12.06
3% $\text{CeO}_2/\gamma\text{-Al}_2\text{O}_3$	128.71	0.40	11.81
6% $\text{CeO}_2/\gamma\text{-Al}_2\text{O}_3$	111.86	0.39	11.64
9% $\text{CeO}_2/\gamma\text{-Al}_2\text{O}_3$	103.25	0.38	11.53
15% $\text{CeO}_2/\gamma\text{-Al}_2\text{O}_3$	75.12	0.35	11.24

controllers (MFCs) (1), and their concentrations in the system were designed according to the range of basal coal-fired flue gas composition: $20.02\text{ }\mu\text{g}/\text{m}^3\text{ Hg}^0$, 5% O_2 , 800 ppm NO , 1000 ppm SO_2 , 10% $\text{H}_2\text{O}(\text{g})$, and balanced with N_2 in the system. The total flux of gas was 1 L/min, and the space velocity (SV) was around $7.6 \times 10^3\text{ h}^{-1}$. The fixed-bed reactor (5) is comprised of a digital temperature controller (3) and a quartz tube with an inner diameter of 10 mm. About 1.0 g of catalyst (4) is packed in the quartz tube, which has been demonstrated to have good chemical resistance and inertness toward mercury. The digital temperature controller (3) was employed to keep the fixed-bed reactor at the desired temperature. The exhaust gas from the mercury analyzer was introduced into the activated carbon trap (6) before being expelled into the atmosphere.

During the experiments, the inlet and outlet Hg^0 concentrations were measured online by the portable mercury analyzer (9) (model QM201G), which was based on cold-vapor atomic fluorescence spectroscopy. The detection limit was $0.001\text{ }\mu\text{g}/\text{m}^3$, and the nominal range was $0.01\text{--}100\text{ }\mu\text{g}/\text{m}^3$. In the Hg^0 analyzer, the sample gas was first dehumidified by silica gel and then entered into the mercury collector, where Hg^0 was collected by the gold film. After collection, the gold film was heated to the desired high temperature to release Hg^0 . Throughout the monitoring processes, the mercury analyzer provided a real-time response every 3 min.

In our study, the inlet Hg^0 concentration was fixed. The experiments were carried out in a batch mode. Before each run, the inlet Hg^0 concentration was measured by closing the valve (14). Then, after opening the valve (14) and closing the valve (13), the gas flowed through the fixed-bed reactor. At this moment, the value of mercury analyzer was the outlet Hg^0 concentration. According to the literature, the Hg^0 removal efficiency (η) is defined as²⁷

$$\eta = \frac{\text{Hg}_{\text{in}}^0 - \text{Hg}_{\text{out}}^0}{\text{Hg}_{\text{in}}^0} \times 100\% \quad (1)$$

where Hg_{in}^0 and Hg_{out}^0 are the Hg^0 inlet and outlet concentrations, respectively.

The error of experiment is inevitable. Hence, the mercury removal points in the figures are the average of three experimental data. The relative errors of experimental results were controlled below 1%.

3. RESULTS AND DISCUSSION

3.1. Characteristics of the Sample. The pore structure parameters of the samples are shown in Table 1. It is obvious that the virgin $\gamma\text{-Al}_2\text{O}_3$ has the highest BET surface area (approximately $141.66\text{ m}^2/\text{g}$) and largest pore size (approximately 12.06 nm). However, the BET surface area, total pore volume, and pore size of the samples decrease with the increase of the CeO_2 loading value. Especially, when the CeO_2 loading value reaches 15%, the BET surface area is sharply reduced from 141.66 to $75.12\text{ m}^2/\text{g}$, the total pore volume is reduced from 0.43 to $0.35\text{ m}^3/\text{g}$, and the pore size changes from 12.06 to 11.24 nm. The reason may be that the active

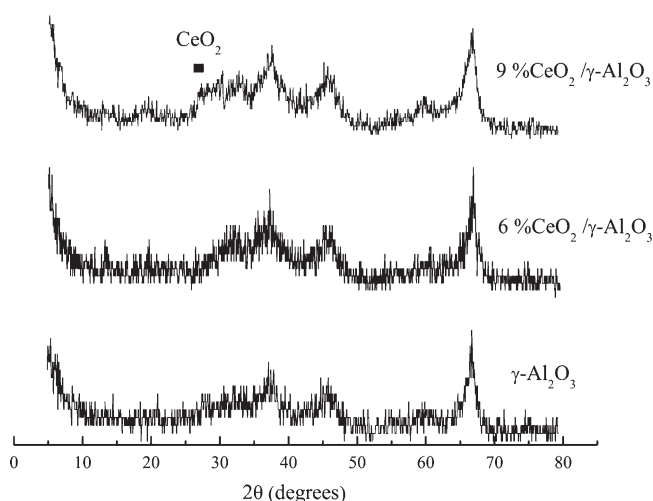


Figure 2. XRD comparison between samples of virgin γ -Al₂O₃, 6% CeO₂/ γ -Al₂O₃, and 9% CeO₂/ γ -Al₂O₃.

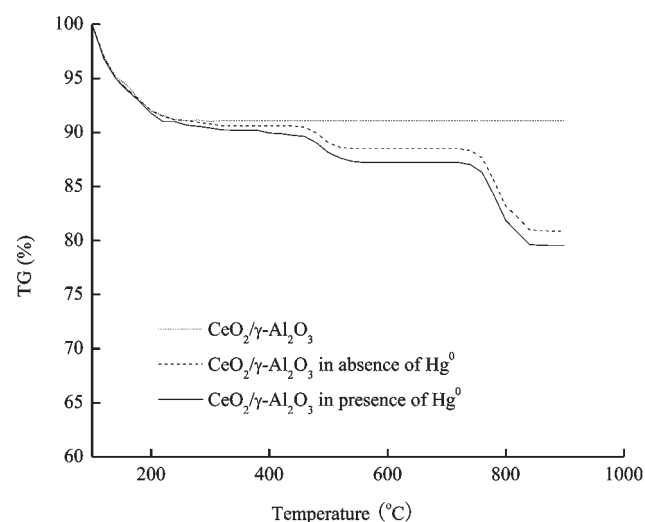


Figure 3. TG analyses of the samples.

component, CeO₂, is impregnated on the surface of γ -Al₂O₃ and blocked its pores.²⁸

Figure 2 shows the XRD patterns of virgin γ -Al₂O₃, 6% CeO₂/ γ -Al₂O₃, and 9% CeO₂/ γ -Al₂O₃. The peaks at the ranges of $2\theta = 36$ – 40° , 44 – 48° , and 65 – 70° in the XRD pattern are corresponding to the characteristic peaks of γ -Al₂O₃, which can be detected in these three samples. Furthermore, there is no CeO₂ characteristic peak for 6% CeO₂/ γ -Al₂O₃. According to the monolayer dispersion theory,²⁹ an oxide like CeO₂ has a trend of spontaneous dispersion on the carrier surface and forms a monolayer or sub-monolayer. This is because, when the oxide content is in the range of the threshold value, the oxide is in a monolayer dispersion state and, when the content of oxide is more than the threshold value, the oxide is in a crystalline phase. The XRD pattern of 9% CeO₂/ γ -Al₂O₃ shows a weak crystal phase of CeO₂, powerfully indicating that the surface of γ -Al₂O₃ is occupied by CeO₂.

TG analyses of fresh CeO₂/ γ -Al₂O₃ and 9% CeO₂/ γ -Al₂O₃, which was used at 350 °C in the presence and absence of Hg⁰ in the flue gas, are shown in Figure 3. There is a quick mass loss as

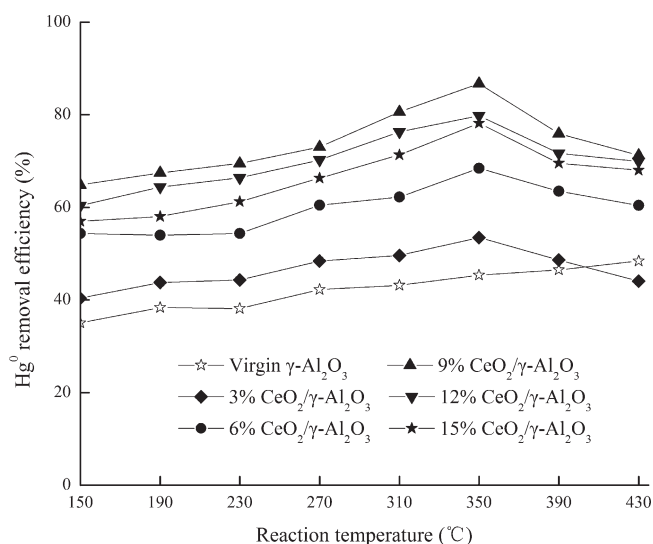


Figure 4. Relationship between the Hg⁰ removal efficiency and CeO₂ loading value supported on γ -Al₂O₃ at different reaction temperatures (reaction time of 1 h).

the temperature increases up to 200 °C for the three curves, which corresponds to the evaporation of adsorbed water. As for the TG curve of used 9% CeO₂/ γ -Al₂O₃ in the presence of Hg⁰ in the flue gas, the small weight loss that occurred at 400 °C can be ascribed to HgO.³⁰ As the pyrolysis temperature increases to 450 °C, the weight losses of used 9% CeO₂/ γ -Al₂O₃, which was used at 350 °C in the presence and absence of Hg⁰ in the flue gas, can be attributed to the decomposition of Ce(SO₄)₂ and their weight loss at 750 °C can be ascribed to the decomposition of Ce₂(SO₄)₃ according to the related research.³¹

3.2. Effects of the Loading Value and Reaction Temperature. Figure 4 presents the relationship between the Hg⁰ removal efficiency and CeO₂ loading value supported on γ -Al₂O₃ at different reaction temperatures (reaction time = 1 h). As shown in this figure, γ -Al₂O₃-loaded 9% CeO₂ shows significantly higher Hg⁰ removal efficiency. At the temperature of 350 °C, with the loading value of CeO₂ changing from 0 to 9 wt %, Hg⁰ removal efficiency increases from 45.36 to 86.76%, which indicates that CeO₂ has an obvious accelerative effect on Hg⁰ removal. Figure 3 illustrates that HgO is the major product of the Hg⁰ removal reaction over CeO₂/ γ -Al₂O₃, indicating that CeO₂ can catalyze the oxidation reaction of Hg⁰.¹⁹ The processes can be described as follows: First, Hg⁰ in the flue gas collides with the catalyst and is adsorbed onto its surface. Then, the adsorbed Hg⁰ is oxidized by the active constituent on the sample surface, leading to the formation of Hg²⁺ presented as HgO. Therefore, the more the CeO₂ loading value, the higher the Hg⁰ removal efficiency of CeO₂/ γ -Al₂O₃. However, the Hg⁰ removal efficiency does not enhance consistently but decreases when the CeO₂ loading value increases above 9 wt %. Especially with a loading value of 15 wt %, the Hg⁰ removal efficiency decreases to 78.17%. The possible reason can be ascribed to the fact that the surface area, total pore volume, and pore size of CeO₂/ γ -Al₂O₃ decrease with the increase of CeO₂, as shown in Table 1. The decrease of the surface area prevents the valid collision between Hg⁰ and CeO₂/ γ -Al₂O₃.³² Although CeO₂ can promote the Hg⁰ removal, its positive effect is weaker than its side effect when the CeO₂ loading is higher than 9 wt %. Therefore, the loading value

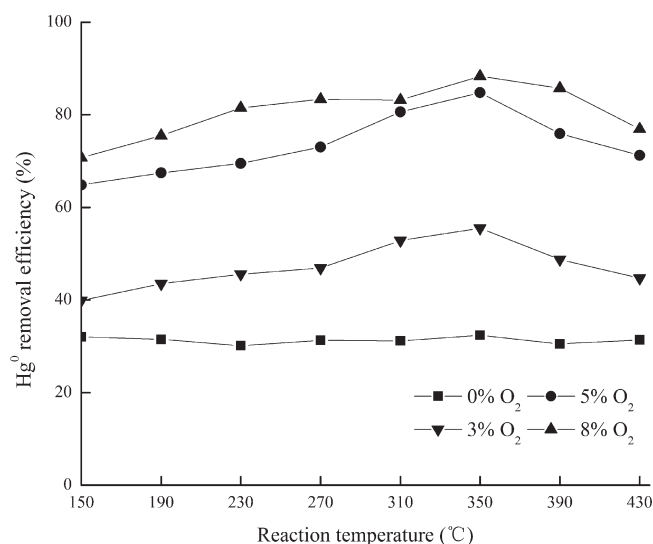
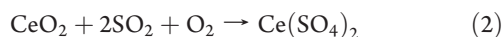


Figure 5. Effect of the O₂ concentration on Hg⁰ removal efficiency at different reaction temperatures (9% CeO₂/γ-Al₂O₃ and reaction time of 1 h).

of CeO₂ supported on γ-Al₂O₃ possesses an optimum value (9 wt % in this paper).

On the other hand, when the CeO₂ loading value is kept constant, the Hg⁰ removal efficiencies increase continuously with the temperature increasing in the range of 150–350 °C. However, when the temperature is over 350 °C, Hg⁰ removal efficiencies decrease slowly, except that of virgin γ-Al₂O₃. This is because, when the temperature exceeds 300 °C, the excessive CeO₂ would react with SO₂ and O₂, forming Ce(SO₄)₂, expressed as³³



The generated Ce(SO₄)₂ covers the surface of γ-Al₂O₃ and blocks its micropores, preventing Hg⁰ from contacting CeO₂. Moreover, with the temperature increasing, the cell size of crystal CeO₂ becomes larger and can also block the pores of γ-Al₂O₃.³⁴ These changes lead to a decrease of Hg⁰ removal efficiency. The Hg⁰ removal efficiency of virgin γ-Al₂O₃ still increases after 300 °C because, as the experimental temperature rises, reactants can obtain more kinetic energy, which enhances the catalytic activity of the samples for the oxidation of Hg⁰.

3.3. Effect of O₂. Figure 5 shows the effects of O₂ on Hg⁰ removal when 0, 3, 5, and 8% O₂ were individually added to the flue gas system of N₂ + O₂ + NO + SO₂ + H₂O (reaction time = 1 h). The results indicate that, in the absence of O₂, only about 30% Hg⁰ removal efficiency is achieved and even lower than that of virgin γ-Al₂O₃ in Figure 4. When O₂ is added to the flue gas, the Hg⁰ removal enhances. The higher concentration of O₂, the higher the removal efficiency. For example, as the O₂ concentration increases to 8%, the Hg⁰ removal efficiency of CeO₂/γ-Al₂O₃ is the highest over the full operating temperature range.

Combing the results of Figures 3 and 5, it is easy to draw a conclusion that O₂ may be the principal active constituent oxidant of the Hg⁰ removal reaction. In the process, a proportion of Hg⁰ is adsorbed by CeO₂/γ-Al₂O₃ and then oxidized directly by O₂ through reaction 3. Another part of Hg⁰ is oxidized by the lattice oxygen stored in CeO₂ through reactions 4 and 5.³⁵ On the basis of Figure 4, the oxidation of Hg⁰ took place mainly

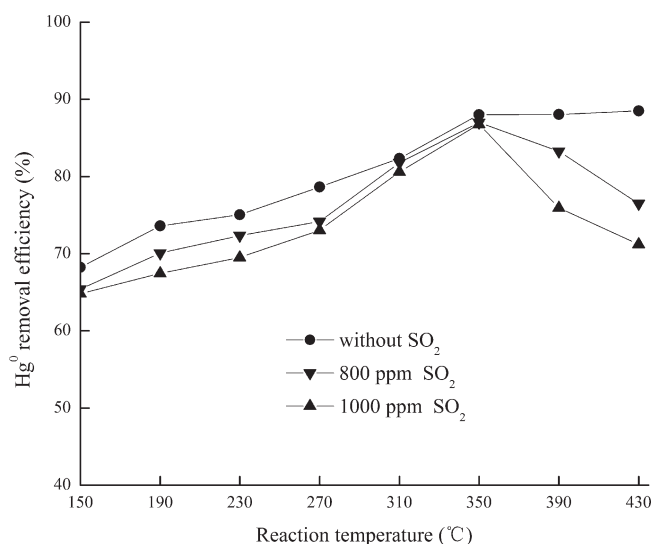
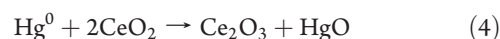


Figure 6. Effect of SO₂ on Hg⁰ removal efficiency at different reaction temperatures (9% CeO₂/γ-Al₂O₃ and reaction time of 1 h).

through reactions 4 and 5 in the presence of CeO₂ because of its catalyst role.



3.4. Effect of SO₂. Figure 6 gives the effects of SO₂ on the Hg⁰ removal efficiency of 9% CeO₂/γ-Al₂O₃ at different reaction temperatures (reaction time = 1 h). The results reveal that SO₂ has an inhibitory effect on Hg⁰ removal of CeO₂/γ-Al₂O₃, especially when the reaction temperature exceeds 350 °C. At the reaction temperature of 430 °C, the Hg⁰ removal efficiency without SO₂ can reach 88.5% but decreases to 72.1% with 1000 ppm SO₂ in the flue gas system of N₂ + O₂ + NO + H₂O. This is because the competitive adsorption between Hg⁰ and SO₂ on the CeO₂/γ-Al₂O₃ surface will occur, and it has an adverse effect on the Hg⁰ removal efficiency. Moreover, when the reaction temperature is below 300 °C, the adsorbed SO₂ could react with O₂ and H₂O to form H₂SO₄, and when the reaction temperature is above 300 °C, reaction 2 can be at work. Both H₂SO₄ and Ce(SO₄)₂ can cover the surface of γ-Al₂O₃ and go against the Hg⁰ removal. Additionally, the result is somewhat different from that by Fan et al.²⁰ and Zhou et al.,³⁶ who reported that the presence of SO₂ can promote Hg⁰ removal. Likely, this difference resulted from different operation conditions. For example, there was no H₂O in their experimental flue gas, which could react with O₂ and SO₂ to form H₂SO₄. Ce(SO₄)₂ was hard to form in the experiment by Fan et al. because of the lower operation temperature (<300 °C). On the other hand, adsorbed SO₂ could react with O₂ to form SO₃, which had strong oxidation ability on Hg⁰; therefore, SO₂ could promote the Hg⁰ removal in their experiments.

3.5. Effect of NO. To investigate the effects of NO on the Hg⁰ removal efficiency, the experiments were carried out with different NO concentrations (0, 800, and 1000 ppm) in the flue gas system of N₂ + O₂ + SO₂ + H₂O using 9% CeO₂/γ-Al₂O₃ at different reaction temperatures. With the reaction time equal to 1 h, the results are presented in Figure 7.

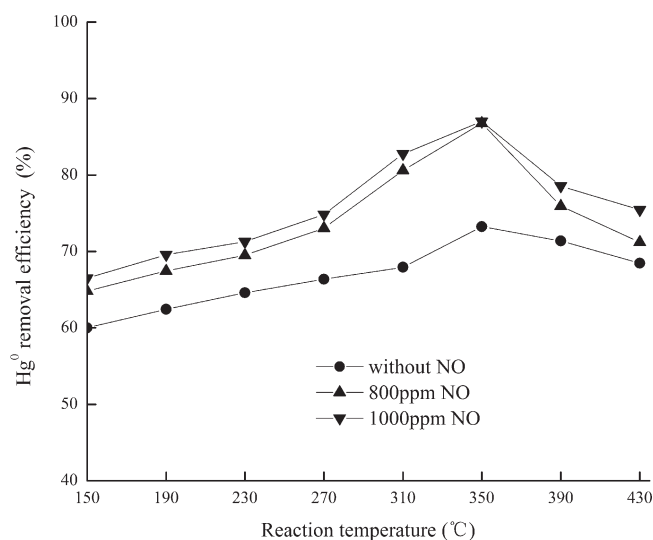
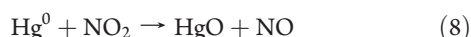
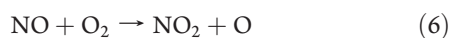


Figure 7. Effect of NO on Hg^0 removal efficiency at different reaction temperatures (9% $\text{CeO}_2/\gamma\text{-Al}_2\text{O}_3$ and reaction time of 1 h).

When NO is 1000 ppm in the flue gas system, the Hg^0 removal efficiency of 9% $\text{CeO}_2/\gamma\text{-Al}_2\text{O}_3$ increases from 73.24 to 86.99% at 350 °C. It indicates that NO has a promotional effect on Hg^0 removal. The possible reason can be ascribed to the following mechanism: Both $\text{Hg}^0(\text{g})$ and NO can be adsorbed by $\gamma\text{-Al}_2\text{O}_3$, but the competition of the two for similar active sites on the surface is minimized.³⁷ In the oxidizing atmosphere, NO is absorbed on the $\text{CeO}_2/\gamma\text{-Al}_2\text{O}_3$ surface and catalyzed by CeO_2 to form NO_2 and O. Meanwhile, $\text{Hg}^0(\text{g})$ can also react with active O and NO_2 to produce HgO .^{36,38–41} The series of reactions can be described as



3.6. Effect of $\text{H}_2\text{O}(\text{g})$. Experiments about effects of $\text{H}_2\text{O}(\text{g})$ on Hg^0 removal were conducted in a relatively dry condition bypassing the water bubbler and in humid conditions. The results are presented in Figure 8 (reaction time = 1 h). Generally speaking, H_2O has a slight inhibitory effect on Hg^0 removal, which agrees with that by Li et al.⁴⁰ As the concentration of $\text{H}_2\text{O}(\text{g})$ increases to 10%, the Hg^0 removal efficiency decreases about 3.51% and even up to 6.07% at 230 °C. The inhibition of H_2O is attributed first to competitive adsorption between Hg^0 and H_2O on the $\text{CeO}_2/\gamma\text{-Al}_2\text{O}_3$ surface. On the other hand, adsorbed H_2O could react with SO_3 to form H_2SO_4 , which covered the surface of $\gamma\text{-Al}_2\text{O}_3$, and go against the Hg^0 removal, but this inhibition would weaken when the reaction temperature is above 320 °C because of the pyrolysis of H_2SO_4 .⁴²

3.7. Effect of the Reaction Time. According to the results of section 3.2, Hg^0 removal efficiencies are highest when using 9% $\text{CeO}_2/\gamma\text{-Al}_2\text{O}_3$ at 350 °C and virgin $\gamma\text{-Al}_2\text{O}_3$ at 430 °C. Therefore, the effect of the reaction time on Hg^0 removal efficiency is studied under these conditions. The results are shown in Figure 9.

As shown in the figure, the Hg^0 removal efficiency of 9% $\text{CeO}_2/\gamma\text{-Al}_2\text{O}_3$ remains constant (about 85%) within 18 h. However, for virgin $\gamma\text{-Al}_2\text{O}_3$, when the reaction time is more than 6 h, its Hg^0 removal efficiency begins to decrease and is about 33.5% at the

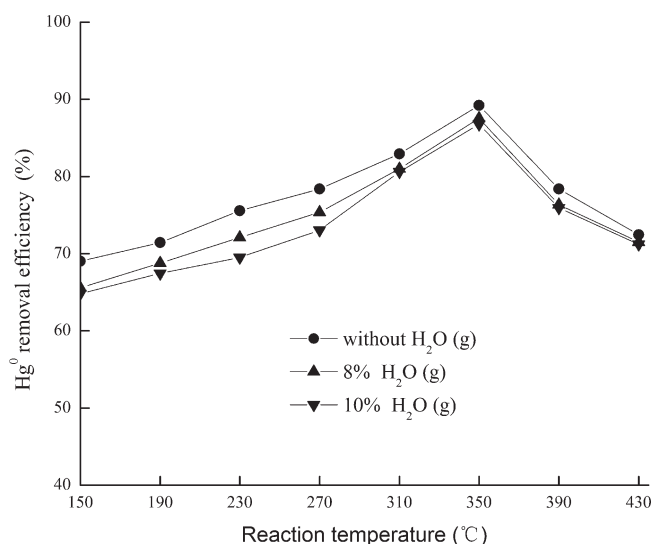


Figure 8. Effects of $\text{H}_2\text{O}(\text{g})$ on Hg^0 removal at different reaction temperatures (9% $\text{CeO}_2/\gamma\text{-Al}_2\text{O}_3$).

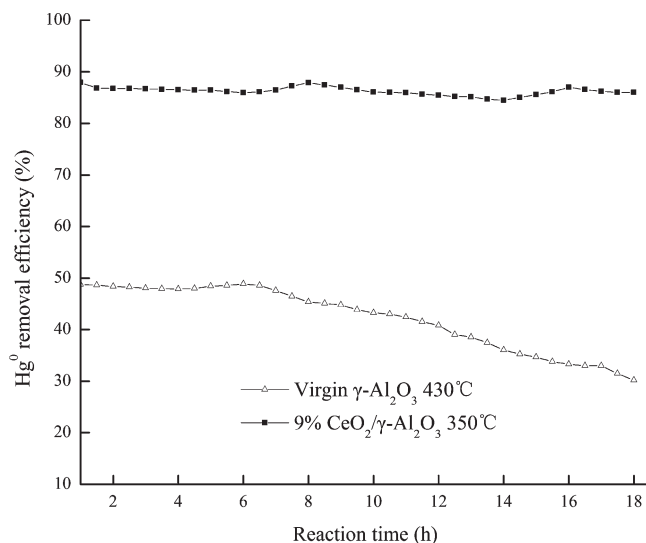
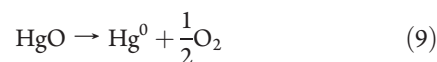


Figure 9. Effect of the reaction time on Hg^0 removal efficiency.

reaction time of 18 h. When the reaction temperature exceeds 400 °C, the reaction 9 is supposed to take place slowly and is heavily dependent upon the amount of HgO on the catalyst surface.³¹ Therefore, the inhibition of reaction 9 is smaller on the Hg^0 removal efficiency of $\gamma\text{-Al}_2\text{O}_3$ at the initial time because of a small quantity of HgO on the surface of the catalyst. With the prolonging of reaction times, more and more HgO is produced, which enhances the inhibition of reaction 9. Therefore, the Hg^0 removal efficiency of virgin $\gamma\text{-Al}_2\text{O}_3$ decreases with the reaction time, especially when the reaction time exceeded 6 h.



4. CONCLUSION

In this work, the removal of Hg^0 was conducted in a lab-scale fixed-bed system over $\text{CeO}_2/\gamma\text{-Al}_2\text{O}_3$ at different reaction

temperatures. The experimental results show that CeO₂ could catalyze the Hg⁰ removal reaction and the Hg⁰ removal efficiency of CeO₂/γ-Al₂O₃ increases with the increase of the CeO₂ loading value. However, when the CeO₂ loading exceeds 9%, the Hg removal efficiency began to decrease. BET analysis shows that the surface area of CeO₂/γ-Al₂O₃ will decrease with the increase of CeO₂ loading values, which prevents the valid collision between Hg⁰ and CeO₂/γ-Al₂O₃ and, thereby, the decrease of Hg⁰ removal efficiency. Therefore, the most suitable loaded mass percentage of CeO₂ is 9%. Moreover, the reaction temperature is an important factor on the Hg⁰ removal of CeO₂/γ-Al₂O₃. With the rise of the experimental temperature, the Hg⁰ removal efficiency increases and then decreases after the reaction temperature is above 350 °C because of the generation of Ce(SO₄)₂, which can prevent Hg⁰ further contacting CeO₂. In the flue gas system of N₂ + O₂ + NO + SO₂ + H₂O, the presence of O₂ and NO has positive effects on the Hg⁰ removal efficiency, while the presence of SO₂ and H₂O(g) has inhibitory effects on the Hg⁰ removal efficiency. Meanwhile, the results testify that the catalyst of CeO₂/γ-Al₂O₃ possesses excellent thermostability within the studied life span.

AUTHOR INFORMATION

Corresponding Author

*Telephone: +86-731-88649216. Fax: +86-731-88649216.
E-mail: cqli@hnu.cn, cqli3@yahoo.com, and/or wenziaoyu1221@126.com.

ACKNOWLEDGMENT

The authors gratefully acknowledge the financial support of the National Natural Science Foundation Project of China (NSFC-50878080 and NSFC-50978088), the Scientific and Technological Major Special Project of Hunan Province in China (2010XK6003), and the Scientific and Technological Major Special Project of Changsha City in China (K0902006-31).

REFERENCES

- Hua, X. Y.; Zhou, J. S.; Li, Q. K.; Luo, Z. Y.; Cen, K. F. *Energy Fuels* **2010**, *24*, 5426–5431.
- Pavlish, J. H.; Sondreal, E. A.; Mann, M. D.; Olson, E. S.; Galbreath, K. C.; Laudal, D. L.; Benson, S. A. *Fuel Process. Technol.* **2003**, *82* (2–3), 89–165.
- Seigneur, C.; Karamchandani, P.; Lonhman, K.; Vijayaraghavan, K.; Shia, R. L. *Geophys. Res. Lett.* **2001**, *106* (27), 795–809.
- United Nations Environment Programme (UNEP)—Chemicals. Mandates for the mercury programme; UNEP—Chemicals: Geneva, Switzerland, 2009; <http://www.chem.unep.ch/mercury/mandates.htm> (accessed on Aug 2010).
- Zhao, B. T.; Zhang, Z. X.; Jin, J.; Pan, W. P. *J. Hazard. Mater.* **2009**, *2–3*, 1179–1185.
- Murakami, A.; Uddin, M. A.; Ochiai, R.; Sasaoka, E.; Wu, S. J. *Energy Fuels* **2010**, *24*, 4241–4249.
- Martinez, A. I.; Deshpande, B. K. *Fuel Process. Technol.* **2007**, *88*, 982–987.
- Korpiel, J. A.; Vidic, R. D. *Environ. Sci. Technol.* **1997**, *31*, 2319–2325.
- Krishnan, S. V.; Gullett, B. K.; Jozewicz, W. *Environ. Sci. Technol.* **1994**, *28*, 1506–1512.
- Krishnan, S. V.; Gullett, B. K.; Jozewicz, W. *Environ. Prog.* **1997**, *16*, 47–53.
- Liu, W.; Vidic, R. D. *Environ. Sci. Technol.* **2000**, *34*, 154–159.
- Wu, S. J.; Uddin, M. A.; Sasaoka, E. *Fuel* **2006**, *85*, 213–218.
- Granite, E. J.; Pennline, H. W.; Hargis, R. A. *Ind. Eng. Chem. Res.* **2000**, *39*, 1020–1029.
- Portzer, J. W.; Albritton, J. R.; Allen, C. C.; Gupta, R. P. *Fuel Process. Technol.* **2004**, *85*, 621–630.
- Presto, A. A.; Granite, E. J. *Environ. Sci. Technol.* **2006**, *40*, 5601–5609.
- Zhao, Y.; Mann, M. D.; Pavlish, J. H.; Mibeck, B. A. F.; Dunham, G. E.; Olson, E. *Environ. Sci. Technol.* **2006**, *40*, 1603–1608.
- Qian, L. W.; Zhu, J.; Du, W. M.; Qian, X. F. *Mater. Chem. Phys.* **2009**, *115*, 835–840.
- Chen, L.; Li, J.; Ge, M. *J. Phys. Chem. C* **2009**, *113*, 21177–21184.
- Gao, X.; Jiang, Y.; Zhong, Y.; Luo, Z.; Cen, K. F. *J. Hazard. Mater.* **2010**, *174*, 734–739.
- Fan, X. P.; Li, C. T.; Zeng, G. M.; Gao, Z.; Chen, L.; Zhang, W.; Gao, H. L. *Energy Fuels* **2010**, *24*, 4250–4254.
- Tian, L. H.; Li, C. T.; Li, Q.; Zeng, G. M.; Gao, Z.; Li, S. H. *Fuel* **2009**, *88*, 1687–1691.
- Reddy, B. M.; Khan, A.; Yamada, Y.; Kobayashi, T.; Loridant, S.; Volta, J. C. *J. Phys. Chem. B* **2003**, *107*, 5162–5167.
- Cai, W. Q.; Li, H. Q.; Zhang, Y. *Colloids and Surf., A* **2007**, *295*, 185–192.
- Zhang, Z. R.; Hicks, R. W.; Pauly, T. R.; Pinnavaia, T. J. *J. Am. Chem. Soc.* **2002**, *124*, 1592.
- Tanaka, K.; Imai, T.; Murakami, T.; Matsumoto, T.; Sugimoto, W.; Takasu, Y. *Chem. Lett.* **2002**, *14*, 2086.
- Qiao, S. H.; Chen, J.; Li, J. F.; Qu, Z.; Yan, N. Q.; Jia, J. Q. *Ind. Eng. Chem. Res.* **2009**, *48*, 3317–3322.
- Lee, S. S.; Lee, J. Y.; Keener, T. C. *J. Chin. Inst. Chem. Eng.* **2008**, *39*, 137–142.
- Lu, P.; Li, C. T.; Zeng, G. M.; He, L. J.; Peng, D. L.; Cui, H. F.; Li, S. H.; Zhai, Y. B. *Appl. Catal., B* **2010**, *96*, 157–161.
- Xie, Y. Ch.; Tang, Y. Q. *Adv. Catal.* **1990**, *37* (17), 1–43.
- Lopez-Anton, M. A.; Yuan, Y.; Perry, R.; Maroto-Valer, M. M. *Fuel* **2010**, *89*, 629–634.
- Yang, Y.; Yang, R. D. *J. Chin. Soc. Rare Earths* **1993**, *4*, 293–296.
- Mei, Z. J.; Shen, Z. M.; Zhao, Q. J.; Wang, W. H.; Zhang, Y. J. *J. Hazard. Mater.* **2008**, *152*, 721–729.
- Yu, Q. C.; Zhang, S. C.; Wang, X. D. *Clean Coal Technol.* **2007**, *13* (3), 74–77 (in Chinese).
- Zhu, H. Y.; Shen, M. M.; Liu, T. D.; Wei, S. T.; Hu, Y. H.; Dong, L.; Chen, Y. *Chin. J. Catal.* **2002**, *4*, 325–328.
- Presto, A. A.; Granite, E. J. *Platinum Met. Rev.* **2008**, *52* (3), 144–154.
- Zhou, J. S.; Luo, Z. Y.; Hu, C. X.; Cen, K. F. *Energy Fuels* **2007**, *21*, 491–495.
- Wang, J. W.; Yang, J. L.; Liu, Z. J. *Fuel Process. Technol.* **2010**, *91*, 676–680.
- Wang, Y. J.; Duan, Y. F.; Yang, L. G.; Zhao, C. S.; Shen, X. L.; Zhang, M. Y. *Fuel Process. Technol.* **2009**, *90*, 643–651.
- Wang, Z. H.; Zhou, J. H.; Zhu, Y. Q.; Wen, Z. C.; Liu, J. Z.; Cen, K. F. *Fuel Process. Technol.* **2007**, *88*, 817–823.
- Li, Y.; Murphy, P.; Wu, C. Y. *Fuel Process. Technol.* **2008**, *89*, 567–573.
- Niksa, S.; Helble, J. J.; Fujiwara, N. *Environ. Sci. Technol.* **2001**, *35*, 3701–3706.
- Li, Y.; Wu, C. Y. *Environ. Sci. Technol.* **2006**, *40*, 6444–6448.